RSC Advances

Optimization of production conditions for synthesis of chemically activated carbon produced from pine cone using response surface methodology for CO2 adsorption

Journal:	*RSC Advances*
Manuscript ID	RA-ART-09-2015-018986.R1
Article Type:	Paper
Date Submitted by the Author:	22-Oct-2015
Complete List of Authors:	Khalili, Soodabeh; Semnan University, Chemical Engineering khoshandam, Behnam; Semnan University Jahanshahi, Mohsen; Babol University of technology,
Subject area & keyword:	Separation science < Analytical

A new insight to the production optimization of activated carbon from pine cone using RSM methodology for CO_2 adsorption.

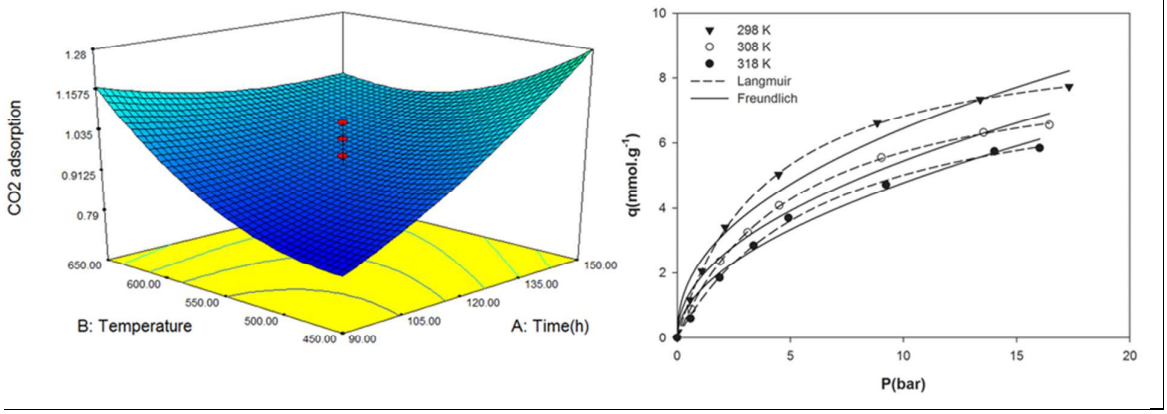

Optimization of production conditions for synthesis of chemically activated carbon produced from pine cone using response surface methodology for CO_2 adsorption

S. Khalili[a], B. Khoshandam[a,*], M. Jahanshahi[b]

[a] Oil, Gas and Chemical Engineering Department, Semnan University, Semnan, Iran.

[b] Nanotechnology Institute, Chemical Engineering Department, Babol University of Technology, Babol, Iran.

[*]Corresponding author

Ph: +98 23 33354120

Fax: +98 23 33354120

Email: bkhoshandam@semnan.ac.ir

P.O. Box: 35195- 363, Semnan, Iran

Abstract

The conditions for the preparation of activated carbon from pine cone for CO_2 adsorption were optimized by response surface methodology (RSM) and central composite design (CCD). The effects of the activation time, activation temperature, and impregnation ratio of H_3PO_4 were studied. The produced activated carbons were characterized by CO_2 adsorption capacity, iodine number and carbon yield. Three quadratic models were developed to correlate the preparation variables for three responses. The experimental data obtained from activated carbon prepared under optimum condition were in good agreement with the values predicted from the models, with relatively small errors between the predicted and the actual values. The prepared activated carbon was characterized by elemental analysis, N_2 adsorption isotherm at 77 K, Fourier transform infrared spectroscopy (FTIR), transmission electron microscopy (TEM) and scanning electron microscopy (SEM). The equilibrium adsorption of CO_2 on prepared AC was experimentally investigated via volumetric method at temperature range of 298–318 K and pressures up to 16 bars. The experimental CO_2 adsorption data were analyzed by Langmuir and Freundlich isotherms models. The adsorption behavior was well described by the Langmuir isotherm model, showing a monolayer adsorption capacity for CO_2 on prepared AC. Results demonstrated that the negative values of heat of adsorption obtained for AC were lower than 80 $kJ.mol^{-1}$ indicating that the interaction between AC and CO_2 molecules is exothermic and physical interactions.

Keywords: Activated carbon, Pine cone, Response surface methodology, Optimization, CO_2 adsorption.

Introduction

Global warming due to CO_2 emissions into the atmosphere has become an environmental issue of great concern, due to its relevant contribution to the global climate change [1, 2].

Many efforts have been done to develop various techniques for CO_2 removal including chemical absorption, physical absorption, physical adsorption, membrane separation, and cryogenic separation [3, 4]. Among the various chemical and physical processes available for CO_2 removal, using aqueous solution of alkanolamines such as monoethanolamine and diethanolamine based absorption method is well known with significant commercial application for CO_2 capture [5, 6]. However, some drawbacks associated with liquid amine solutions for CO_2 separation such as extensive corrosion of equipment, high cost of amine, oxidative solvent degradation, large energy penalty for regeneration and loss of amine during regeneration are reasons which make it indispensable to see other alternative processes [7, 8].

In the recent years, pressure Swing Adsorption (PSA) process by using solid sorbents has gained wide attention in chemical industries for CO_2 separation. It has become a promising technology for CO_2 capture due to low cost, high selectivity, high adsorption capacity, easy regeneration of adsorbents and ease of applicability over a relatively wide range of temperatures and pressures [9, 10].

A large number of solid materials have been investigated lately as potential adsorbents for CO_2 capture, which includes activated carbons, zeolites, mesoporous silicas, carbon nanotubes and metal-organic frame works [11-15].

Among solid sorbents, carbonaceous materials have been used as a potential economical source for CO_2 capture. Activated carbon is an extremely versatile carbonaceous substance that is widely used as adsorbent in industrial wastewater and gas treatment [16]. High surface

area, fast adsorption/desorption kinetics, large pore volume, favorable pore size distribution, surface chemistry including the oxygen functional groups, the degree of polarity, the active surface area and low density are the advantages of activated carbons that render them as appropriate adsorbents for CO_2 adsorption [17-19].

The precursor activators and the production techniques of activated carbon are effective on the adsorption efficiency and cost of activated carbons. Due to the use of non-renewable and expensive starting materials such as natural coal and conventional long duration heating production methods, commercial activated carbons are still considered as relatively expensive materials [20, 21]. Therefore, it is necessary to find low-cost, locally available and renewable materials as potential alternative precursors in activated carbon production. In recent years, biological materials such as fruit stones [22], pyrolyzed coffee residues [23], nutshells [24], olive stones [25] and coconut shell [26] are considered as precursors for preparation of activated carbons due to their low cost and high adsorption capacity. But there are only few studies about application of pine cone in preparation of activated carbon as precursors [27].

Pine cone is one of these low cost agricultural by-products which can be found in large amounts and in various species in pine plantations for the pulp and paper industry with little or no use.

In principle, the preparation of activated carbon is employed by physical or chemical activation methods to enhance their adsorption capacity. In physical activation, the raw material is first carbonized, under an inert atmosphere and the carbonized material is secondarily activated by steam or carbon dioxide. In chemical activation, the raw material is firstly mixed or impregnated by chemical agents such as H_3PO_4, H_2SO_4, $ZnCl_2$, KOH, or K_2CO_3 followed by thermal activation to create the pore structure. In comparison with physical activation, chemical activation does not require as high temperatures [28, 29].

Phosphoric acid activation of lignocellulosic materials has become an increasingly used technique for the large-scale production of activated carbons because of environmental advantages and several other benefits such as facility of recovery (only washing with water) as compared to $ZnCl_2$ activation, low energy cost, and high char yield over the physical activation. Phosphoric acid plays important role in the acid-catalyzed conversion of lignocellulosic materials into a highly porous activated carbon [30, 31].

In order to optimize the experimental synthesis conditions of a wide variety of materials, multivariate statistical techniques can be employed. Among these optimization techniques, response surface methodology (RSM) is the most popular tool in process optimization, consequently, the most applied [32]. This technique is a collection of statistical and mathematical techniques based on the fit of a polynomial equation to the experimental data. When a response or a set of responses of interest are influenced by several variables, response surface methodology can be well applied [33]. Among the second-order symmetrical models applied in analytical techniques, central composite design (CCD) has been widely used in various scientific areas [34].

To the best of our knowledge, no study has been done on optimization of the production of activated carbon from pine cone using the response surface methodology (RSM) approach. Though RSM is a popular tool in process optimization, its application in activated carbon production and used for CO_2 is very limited. Also, employing of pine cone- based activated carbon for CO_2 adsorption can be considered as an another new aspect of this work. Therefore, the main objective of this study was to apply CCD to optimize the production of AC from pine cone chemically activated with H_3PO_4. Activation time, activation temperature and impregnation ratio determined as the main three influencing factors were selected as the activated carbon regeneration variables for experiments. Desirable production outputs based on CO_2 adsorption capacity, iodine number and yield of activated carbons were considered as

responses. The iodine number is one of the most popular parameter used as adsorbate standard to measure the surface area of the prepared activated carbons, approximately. Since the specific surface area and the micropore volume are strongly effective in gas adsorption, CO_2 adsorption and iodine number were used as responses for determination of micropore volume and specific surface area, respectively.

2. Materials and methods

2.1 materials

Pine cone was used as a raw material for preparation of activated carbons. This precursor was collected from Semnan province, Iran. Carbon dioxide, helium and Nitrogen with purity of 99.99%, 99.995% and 99.995% were obtained from Technical Gas Services, UAE.

Hydrochloric acid 37% (HCl), phosphoric acid 85% (H_3PO_4) were obtained from scharlau. Also distilled water was used throughout this work.

2.2 Preparation of activated carbon

Pine cones collected from Semnan was first washed with distilled water several times to remove the impurities (dust and water soluble substances) and then dried in an oven overnight at 110 ^{0}C to remove the moisture and other volatile impurities.

The washed cones were cut into small pieces and sieved through the mesh number 60. Chemical activation of the precursor was done with impregnating of the precursor with H_3PO_4. 10 g of the dried precursor was impregnated with 85 wt.% H_3PO_4 solution in the different weight ratio and mixed at 80 °C for 3 h. The impregnation ratio is determined as the

ratio of weight of 100% phosphoric acid used for impregnation to the weight of the dry precursor. After mixing, the slurry was placed in the vacuum drying at 110 ^{0}C for 20 h. Impregnated precursor was placed in tubular quartz reactor and subjected to heat treatment at a rate of 5 ^{0}C/min in an electrical furnace for different carbonization times under a nitrogen flow rate of 100 ml/min STP. After pyrolysis, the activated carbon was cooled down to room temperature in a flow of nitrogen and then removed from the reactor. In all experiments, nitrogen flow rate and heating rate were kept constant. Pyrolysis under inert gas breaks down the cross-link between carbon atoms and avoids the dilution of gas products.

The products were washed sequentially with 0.5 M HCl solution to remove the activating agent from the material. The AC was separated from the solution by filtration and was washed several times with hot and finally cold distilled water until the pH of the filtrate reached around 6.0 and then dried overnight at 110 ^{0}C and placed in a desiccator.

The activated carbon yield percentage (Y) which is the efficiency of activation process is the amount of activated carbon produced at the end of the activation step and determined by Eq. (1) as follows [35]:

$$Y = \frac{M}{M_0} * 100 \qquad (1)$$

where M (g) is the dry mass of final activated carbon produced after chemical activation and acid wash completed and M_0 (g) is the dry mass of precursor.

2.3 Characterization

The Moisture, volatile matter and ash content of the precursor and prepared activated carbon were determined using a standard method according to ASTM D2867, ASTM D5832-98 and

ASTM D2866-94, respectively. Also adsorption capacity, measured as iodine number which shown milligrams of iodine adsorbed by a gram of activated carbon was define according to ASTM standard D 4607-94 procedure. The Chemical composition of raw pine cone and prepared activated carbon were determined using CHNS elemental analyzer (Costech ECS 4010, Italy).

The morphology of AC was analyzed by TEM (Zeiss EM10C, Germany) at an acceleration voltage of 80 kV and SEM (VEGA II LMU, Tescan, Czech Republic) to obtain supplementary information regarding the AC.

The surface chemistry of the sorbent was evaluated by FTIR spectrometer (Bruker Vertex-70, Germany). Sample disc was prepared by mixing 1mg of the powdered AC with 300 mg of KBr and scanned in the range of 400–4000 cm^{-1}. The textural characterization of the selected activated carbon such as surface area, average pore diameter and pore volume were measured by using an adsorption apparatus (BELSORP 28, BEL Japan Inc.) employing N_2 adsorption–desorption isotherm at 77 K at the relative pressure (P/P_0) range of 0.0001–0.99. Prior to BET analysis, sorbent was separately degassed under vacuum environment at 393 K for 15 h before the nitrogen adsorption measurements.

2.4 Design of experiment using Central Composite Design

The optimal conditions in the production of activated carbon from pine cone were determined by a standard RSM design called central composite design (CCD). Accordingly, in this study, Design-Expert 8.0.5 software was employed to generate experimental designs, statistical analyses, and regression models.

The number of tests development for the CCD consists of the standard 2^n factorial with its origin at the center, 2n points fixed axially at a distance, say α from the center to generate the quadratic terms, and replicate tests at the center. Hence, the full design matrix for the three variables, including 8 factorial points, 6 axial points and 6 replicates at the center points, were used and a total of 20 experiments were obtained from the following equation:

$$N = 2^n + 2n + n_c = 2^3 + 2*3 + 6 = 20 \quad (2)$$

where n is the number of factors and N is the total number of experiments required for CCD [36]. The center points are employed to define the experimental error and the reproducibility of the data. The independent variables are coded as -1, 0, +1 interval which shows the low, center and high level of each variable, respectively. The axial points are placed at (± α, 0, 0), (0, ±α, 0) and (0, 0, ±α) where α is the axial point distance from center and makes the design rotatable. In this study, the value of α was selected 1.682 (rotatable). Table 1 shows the complete design matrix of the experiments performed, together with the results obtained.

By studying three independent variables which are activation time, activation temperature and impregnation ratio at five levels, the CO_2 adsorption capacity, iodine number and carbon yield of activated carbons as three responses were simultaneously optimized.

For RSM, the most commonly used second-degree polynomial model developed to fit the experimental data can be described in the form of the following equation.

$$Y = \beta_0 + \sum \beta_i X_i + \sum \beta_{ii} X^2{}_i + \sum \beta_{ij} X_i X_j + \varepsilon \quad (3)$$

where Y is the predicted response, X_i and Xj represent the coded values of independent variables, β_0 is the constant coefficient, β_i is the linear coefficients, β_{ii} is the quadratic coefficients, β_{ij} is the interaction coefficients and ε is the error of the model.

2.5 CO_2 adsorption measurement

The CO_2 adsorption experiments on the prepared samples were done by using a volumetric adsorption set up. The schematic design of the volumetric adsorption system is shown in Fig. 1. The apparatus included two high-pressure stainless steel pressure and sample cells. Both cells were placed in a thermostatic water bath along with a water circulating system to keep the temperature constant during the CO_2 adsorption experiment.

In order to control gas entrance, the pressure cell was connected to a high-pressure reservoir via a regulator and a needle valve. Before starting each test, the set up was leak-free using pressurized air for 24 hours. Prior to CO_2 exposure, the adsorption cell was cleaned and the adsorbent, which was degassed at 423 K for 24 hours, was put in it. The system was evacuated by vacuum pump for 2 hours. In addition the He gas was employed as non-adsorbing gas to determine the dead volume by using a calibration cell with a definite volume. The exact volume of pressure and sample cells with their connection lines such as tubes and valves were determined with this method. The CO_2 adsorption experiments were initiated by opening the valves between pressure and sample cells and allowing CO_2 gas to enter to the sample cell loaded with the adsorbent. Prepared samples start to adsorb CO_2 gas and a pressure drop was observed until they did not adsorb CO_2 any more.

The amount of adsorbed gas was determined using material balance before and after each test and Soave-Redlich-Kwong (SRK) equation of state for the compressibility factor:

$$\left.\frac{PV}{ZRT}\right|_{L_1} + \left.\frac{PV}{ZRT}\right|_{a_1} = \left.\frac{PV}{ZRT}\right|_{L_2} + \left.\frac{PV}{ZRT}\right|_{a_2} + N \qquad (4)$$

where subscripts 1, 2, L and a refer the initial state, final equilibrium state, pressure cell and sample cell, respectively. Furthermore P is the pressure, V is the volume, Z is the CO_2 compressibility factor, R is the universal gas constant and T is the temperature.

2.6 Adsorption isotherms

The Langmuir isotherm theory [37] assumes monolayer coverage of adsorbate on a homogenous adsorbent surface. This model is described by the following relationship:

$$q = q_m \frac{bP}{1+bP} \quad (5)$$

where q_m and b are Langmuir constants related to the maximum adsorption capacity and energy of adsorption, respectively.

The Freundlich adsorption isotherm is used for non ideal sorption on heterogeneous surfaces [38] and is commonly described by the following nonlinear Equation:

$$q = KP^{\frac{1}{n}} \quad (6)$$

where 1/n is the heterogeneity factor and K is Freundlich constant. For n >1, adsorbate is favorably adsorbed on the adsorbent .

2.7 Thermodynamic of adsorption

The isosteric heat of adsorption of a gas is defined from temperature dependence of the isotherm using the Clausius–Clapeyron equation as follows:

$$\Delta H_{st} = R\left[\frac{d\ln P}{d(\frac{1}{T})}\right]_q \quad (7)$$

where ΔH_{st} (kJ/mol) and P (bar) are isosteric heat of absorption and the pressure at a constant adsorbate loading of q, respectively. R (J/mol.K) is the ideal gas constant and T (K) is the temperature.

In order to evaluate the influence of temperature on adsorption process, the other thermodynamic parameters, such as standard free energy (ΔG), enthalpy (isosteric heat of adsorption under isothermal conditions, ΔH) and entropy of adsorption (ΔS) were estimated from the adsorption data using the following equations [39]:

$$\Delta G = RT\ln\frac{P}{P_s} \quad (8)$$

$$\Delta G = \Delta H - T\Delta S \quad (9)$$

where P is the equilibrium pressure of the adsorbate and P_S is the equilibrium pressure of the adsorbate at standard pressure (1bar).

3. Results and discussion

3.1 Raw material characterization

The results of proximate and ultimate analyses performed on the pine cone (dry basis) are shown in Table 2. The high content of volatile matter, high carbon content and low amount of ash recommended that this precursor is appropriate to obtain activated carbon.

3.2 RSM approach and statistical analysis

Central composite design (CCD) was used to develop correlation between the activated carbon preparation variables to the CO_2 adsorption, iodine number and yield. The complete design matrix for experimental and predicted response values are given in Table 1. Runs 15-20 at the center point were used to determine the experimental error and the reproducibility of the data. According to the sequential model sum of squares, the highest order polynomials were used to select the models where the additional terms were significant and the models were not aliased. For all three responses of CO_2 adsorption, iodine number and yield, the quadratic models were selected, as suggested by the software.

The final empirica regression models in terms of coded factors for adsorption of CO_2 (Y_1), iodine adsorption capacity (Y_2) and carbon yield (Y_3) were defined as follows:

$$\begin{aligned} Y_1 &= 0.95 + 0.100\ X_1 + 0.043\ X_2 - 0.24\ X_3 - 0.14\ X_1\ X_2 \\ &+ 0.11\ X_1\ X_3 - 0.089\ X_2\ X_3 + 0.037\ X_1^2 + 0.094\ X_2^2 + 0.25\ X_3^2 \end{aligned} \quad (10)$$

$$\begin{aligned} Y_2 &= 1319.80 + 20.79X_1 + 1.84X_2 + 9.45X_3 - 7.75X_1X_2 \\ &- 8.75X_1X_3 - 3.25X_2X_3 - 5X_1^2 + 19.39X_2^2 - 11.9X_3^2 \end{aligned} \quad (11)$$

$$\begin{aligned} Y_3 &= 56.42 - 1.56X_1 - 1.38X_2 + 1.05X_3 + 1.93X_1X_2 \\ &+ 1.58X_1X_3 + 0.64X_2X_3 - 0.32X_1^2 - 3.36X_2^2 - 1.41X_3^2 \end{aligned} \quad (12)$$

Positive sign in front of the terms represents synergistic effect whereas the negative sign indicates antagonistic effect**.** The quality of the model developed was considered based on the correlation coefficients value (R^2) and were 0.979, 0.966 and 0.972 for Eqs. (10), (11) and (12), respectively. All three of the R^2 values of CO_2 adsorption, iodine number and carbon

yield were relatively high, representing a good agreement between the experimental data and predicted value from this model.

An analysis of variance (ANOVA) was employed to justify the significance and adequacy of the applied model and identify the actual relationship between the response and significant variables represented by the equation. The significant quadratic models for all responses and analyzed by ANOVA are tabulated in Table 3.

Regression coefficients, the significance and standard error of each coefficient are verified by the values of p and F. The smaller magnitude of p and the larger value of F show that most of the variation in the response can be interpreted by the regression equation. Actually, the associated p value is applied to estimate whether F is large enough to indicate statistical significance. The p value less than 0.05 and greater than 0.1 indicates that the model terms are statistically significant and not significant, respectively [40].

As can be seen in Fig. 2, the experimental values for all responses were in good agreement with the amounts predicted by the model. In Fig.2a the predicted value obtained was more close to the experimental values due to have high R^2.

3.3 CO_2 adsorption capacity

Less CO_2 adsorption capacity is expected when the adsorbent has low surface area and lacks well developed pores, as well as the adsorbent with high percentage of mesopore and macropores. Therefore, CO_2 adsorption in activated carbons not only depends on the development in porosity, but also on the width of micropores. Therefore CO_2 adsorption capacity is favored by high surface areas and high micropore volumes [41].

According to the ANOVA (table 3) for response surface quadratic model for CO_2 adsorption capacity, the model F-value of 50.834 implied that the model was significant. In addition, activation time (X_1), temperature (X_2) and chemical impregnation ratio (X_3) and also the interaction terms were all significant model terms for the CO_2 adsorption with p-values less than 0.05. Adequate precision evaluates the signal-to-noise ratio and compares the range of the predicted values at the design points to the average prediction error. The adequate precision ratios of 25.788, 19.352 and 20.247, derived for the CO_2 adsorption, iodine number and carbon yield, respectively, are much greater than 4 and indicate adequate model discrimination.

Based on the F-value, all the three parameters chosen in this study were found to have significant effects on the CO_2 adsorption pine cone-based activated carbon. The impregnation ratio (X_3) showed the greatest significant effect on this response, with the highest F value of 157.757, while temperature showed slight effect on the response for CO_2 adsorption. The best way to recognize the relation between the factors and response is examination of surface plots as function of two factors by holding the other factor at constant level. The three-dimensional response surfaces graphs for CO_2 adsorption was depicted in Fig. 3. Fig. 3 (a-c) shows that by increasing both temperature and activation time, the CO_2 adsorption response increases. This is perhaps due to this fact that an increase in the activation temperature and activation time cause to increase the formation of micropores which is more effective in CO_2 adsorption process. The formation of micropores may be attributable to this fact that during the carbonization processes the pores are filled with the tarry matter or the products of decomposition or at least blocked partially by disorganized carbon. By increasing the activation temperature and activation time, pore opening is occurred due to the driving off the tar in gaseous form that was trapped in the porous structure and also releasing of other volatile components. Another probable explanation for the formation of the micropores is

that increasing of activation temperature and time led to incorporation of more Phosphorus into the carbonaceous precursors in the form of phosphates or polyphosphates. After removing these components from the precursors, more micropores were created [42, 43]. A decrease in CO_2 adsorption capacity with an increase in impregnation ratio can be observed. Furthermore, the negative sign in front of the (X_3) in Eqs. (7) also indicates its unfavorable or antagonistic effect on the adsorption performance. More increase in the concentration of the activation agent perhaps leads to the excessive dehydration and the destruction of prepared activated carbon micropores and turning them to larger pores which reduces the CO_2 adsorption efficiency.

3.4 Iodine adsorption capacity

As mentioned earlier in CO_2 adsorption process, the most significant features of the prepared adsorbent are their surface area and the porosity which are developed during activation and influenced by the impregnation ratio. Iodine number may be used as an approximation of surface area for activated carbons [44].

For iodine number values of P less than 0.05 from the ANOVA indicated that the model terms were significant. In this case, except X_2 and X_2X_3 which were insignificant to the response of iodine number, all the quadratic terms were significant to the response. Fig. 4 a-c demonstrates the three-dimensional response surfaces which were constructed to show the effects of the activated carbon preparation variables on the I_2 adsorption.

With regard to the adsorption of I_2, activation time is found to have the greatest significant effect (F-value = 97.435) on it among all the three factors (activation time, activation temperature and impregnation ratio) studied, as shown in Fig. 3a and b. The longer activation

time led to release of other high-molecular-weight volatiles which cause to develop more active sites and more pores inside the samples and as a result the I_2 adsorption capacity was increased [45, 46]. According to Fig. 4a and c and F-value of 0.767, activation temperature showed very slight effect on the response for I_2 adsorption.

As seen from Fig. 4b, the iodine number increased with the increase of phosphoric acid concentration due to the fact that phosphoric acid occupied a volume which hinderes the shrinkage of the particle during the heat treatment, therefore leading to the formation of porosity when it is extracted by washing after carbonization [47].

3.5 Carbon yield

Relatively high product yields are expected for economical feasibility in the production of commercial activated carbons. In this study, the model terms such as X_2X_3 and X_1^2 whose values of p are higher than 0.05 in table 3, are not significant whereas all the other quadratic terms were significant to the response. Based on the F-value, activation time has significant effect on AC yield. The effect of activation time on yield of activated carbon is shown in Fig.5a.

The increasing in activation time would cause to release more volatile matter and as a result, reduce the amount of carbon yield. Similar results can be found in Azmi et al. [48] work. It can be seen from Fig. 5b and c that adding chemical agents to the precursor increase the yield of the carbon products. The reduction in weight loss is most likely due to the condensation (polymerization) reactions caused by the chemical agent. These reactions occur among the aromatic hydrocarbons and tar-forming compounds and cause to form larger molecules (polycyclic aromatics) in the structure of activated products and increase the activated carbon

yield [35]. As seen from Fig. 5c, the carbon yield gradually increased with the increase of activation temperature firstly, with the maximum yield of about 57.65% and then rapidly decreased with further increasing temperature from 550 to 650 ^{0}C due to devolatilization of the pine cone upon heating and as expected, the quantity of volatiles evolved increased.

3.6 Process optimization

The main aim of this work was to determine the optimum process parameters to prepare activated carbon from pine cone with high micropore volume (by measuring CO_2 adsorption), high surface area (by measuring I_2 adsorption) and high product yields for economic feasibility. However, as previously mentioned, all three responses showed different interest region under the same condition. In order to compromise between these responses, the function of desirability was applied to find combination of levels of process parameters that produce the maximum desirable response. The activated carbon was prepared under the optimum experimental conditions given in Table 4, together with the predicted and experimental values of CO_2 adsorption at 298 K and 1 bar, iodine number and carbon yield.

The optimum activated carbon showed CO_2 and I_2 adsorption of 1.91 mmol/g and 1345 mg/g, respectively and activated carbon yield of 51.8 %**.** It was observed that the experimental data obtained from AC prepared at optimum condition were in good agreement with the values predicted from the models, with relatively small errors between the predicted and the actual values, which were only 1.57, 1.34 and 2.38 for CO_2 adsorption, iodine number and carbon yield, respectively.

3.7 Characterization of activated carbon prepared under optimum conditions

3.7.1 Ultimate and proximate analysis

Table 2 shows the results of ultimate and proximate analysis of the activated carbon produced from pine cone under optimum conditions. As can be seen from Table 2, after activation, the fixed carbon percent of activated carbon increased and percent of volatile matter decreased.

The elemental analysis of AC show an increase in carbon level but the content of oxygen indicated an opposite trend. This is due to the partial decomposition of volatile compounds and degradation of organic materials under carbonization leaving a high purity carbon.

3.7.2 Surface morphology analysis

The SEM photograph of the prepared activated carbon is shown in Fig.6 a. The figure reveals the porous structure of samples with different size and shapes indicating relatively high surface areas. It seems that the cavities on the surfaces of activated carbon resulted from the evaporation of the phosphoric acid during carbonization, leaving the empty space previously occupied by the activating agent. Fig. 6 b depicts the TEM image of the pine cone-based activated carbon. Obviously, the activated carbon has a well-developed porous structure consisting of worm-like micropores which are formed by the stacking of curved graphene layers.

3.7.3 Porous structure analysis

Fig. 7 shows the N_2 adsorption–desorption isotherms of the activated carbon produced under the optimal conditions from pine cone. It can be seen from Fig. 7 that the AC demonstrates the type I isotherm according to the Brunauer classification, indicating that there are mainly

micropores and a relatively small external surface area in the sample prepared under optimum condition. The most uptake of N_2 adsorption was determined in at low relative pressures region, which is considered due to the formation of highly microporous material with narrow pore-size distribution and monolayer adsorption on the AC. This was previously confirmed by TEM analysis as shown in Fig. 6b

The micropore and mesopore size distributions of AC derived from (a) a Micropore (MP) plot and (b) a Barrete Joynere Halenda (BJH) plot was shown in Fig. 8. The volume distribution (dV_p/dr_p) of AC, especially near to the micropore region increases which indicateds that the prepared AC has mainly micropores with sizes in the ranges of 0.2–1.2 nm and also has some mesopores. Textural parameters of the prepared activated carbon were shown in table 5.

3.7.4 FTIR analysis

The FTIR spectra of pine cone activated carbon is shown in Fig. 9. The peak at 1562 cm^{-1} is assigned to C=C bond in aromatic rings of carbon structure of activated carbon. The peak at 1032 cm^{-1} is assigned to C–O–C stretching that may present in ethers. The C=O bond stretching in lactones can be found at 1704 cm^{-1}. The peaks at 2852 and 2926 cm^{-1} are assigned to asymmetric and symmetric stretching vibrations of –CH group of carboxylic acids. The peak at 2360 cm^{-1} may be assigned to C≡C bond in ketene groups. The appearance of peak at 3430 cm^{-1} is due to the O–H group of phenol, alcohol, and carboxylic acid [49, 50].

3.8 CO_2 adsorption isotherm simulation on prepared AC under optimum conditions

The prepared activated carbon which were produced under optimum condition with high BET specific surface area, were tested in a gas adsorption system. The effect of temperature and pressure were studied on the prepared AC adsorption capacity. Adsorption isotherms of carbon dioxide were conducted at different pressures up to 16 bar and three temperatures, i.e., 298, 308 and 318 K. Fig.10 illustrates the experimental CO_2 adsorption isotherms for prepared AC at different temperatures. All of the CO_2 adsorption isotherms are Type I according to the Brunauer classification, which is expected for adsorption of small adsorbates on a microporous adsorbent [51].

Results demonstrated that at any given temperature, the amount of CO_2 adsorbed on sample is only a function of pressure. It is clearly seen that by increasing the pressure and decreasing the temperature, CO_2 uptake increased. The adsorption isotherms for carbon dioxide indicate that the availability of adsorption sites decreases faster when the adsorptive pressure is increased, due to a stronger adsorbate-adsorbent interaction. Also with increasing CO_2 pressure, the most active sites will be occupied. Thus the surface becomes saturated.

Increasing the temperature leads to decrease the kinetic diameters of the adsorbed molecules and the rate of diffusion into inner sample cavities. In the other words, adsorbed gas molecules obtain sufficient energy to overcome the van der Waals forces and move back to the gas phase. Therefore the sorption values reduce with increasing temperatures.

As it was mentioned before the specific surface area and the micropore volume are strongly effective in gas adsorption. Normally, in the gas–solid interaction the gas molecules are adsorbed by strong van der Waals forces. When the gas molecules start to overlap with the decreasing pore size, the gas adsorption potential in sub-nanometer pores is highest, leading to a much higher binding energy emanating from the formation of deep potential wells.

Therefore, maximization of the sub-nanometer pores number is essential, which automatically causes to an increase in specific surface area [52].

The CO_2 adsorption data onto prepared AC were fitted by common and practical standard isotherm models, Langmuir and Freundlich, respectively. The values of Langmuir and Freundlich isotherm parameters are shown in Table 6.

The comparison of the R^2 values from Table 6 shows that Langmuir isotherm model yields a better fit to the experimental data ($R^2 > 0.99$). It means that at least within the studied temperature ranges, the adsorption of CO_2 onto AC is limited to monolayer coverage with no important interaction among neighboring adsorbed molecules. With increasing the temperature, Langmuir parameters (q_m and K_L) decreased indicating that the affinity between CO_2 and adsorbent had an inverse relationship with temperature confirming an exothermic nature of the adsorption process. As the temperature increased from 298 to 318 K, the K value of the CO_2 adsorbed by AC decreased. These results demonstrated that the adsorption of the CO_2 by AC is more favorable at low temperature, and agreed with the results from the Langmuir isotherm. The Freundlich exponents n values were more than 1, indicating that CO_2 were favorably adsorbed onto prepared AC at all temperatures.

3.9 Thermodynamic of adsorption

Determination of the heat of adsorption and its variation with coverage can give practical information about surface characteristics and the adsorbed phase. Surface characteristics are measurable by determining the heat of adsorption released from the interaction of adsorbate with the adsorbent at a certain loading.

The isosteric heat of adsorption of CO_2 onto prepared AC under optimum conditions was derived from the slope of the plot of lnP versus 1/T at a constant adsorbed amount. Fig. 11 illustrates the variation of calculated heat of adsorption with different constant surface loading. The heat of adsorption is interpreted as an indicator of the interaction strength between the gas molecules and the adsorbent. For heat of adsorption of 80 kJ/mole or more, the adsorption process is chemisorption and smaller values are representative of physisorption [53].

In Fig. 11, the isosteric heat of adsorption for Ac is shown as a function of loading. According to the ideal Langmuir model, the heat of adsorption is independent from surface coverage. However, this necessity is seldom satisfied in actual systems due to the surface heterogeneity and strong effects of adsorbate - adsorbate interaction.

At lower surface coverage, the isosteric heat of adsorption of CO_2 exhibits almost constant, thereby indicating a homogeneous adsorption system and there is no lateral interaction between the adsorbed CO_2 molecules. By increasing CO_2 loading, the isosteric heat of adsorption of CO_2 increases slightly, suggesting that adsorbate–adsorbate interactions are more pronounced in the high-pressure range. The adsorbent–adsorbate interaction happens initially at lower surface coverage, while adsorbate–adsorbate interaction occurs with an increasing of the surface coverage [54]. In the present study, the values of isosteric heat of adsorption obtained for AC were lower than 80 $kJ.mol^{-1}$ indicating that the interaction between AC and CO_2 molecules is mainly physical interactions involving weak van derWaals and electrostatic interactions.

The values of thermodynamic parameters for adsorption of CO_2 onto AC were determined from the slopes and intercepts of the plots of ΔG versus T and the results were listed in Table 7. The Gibbs free energy change (ΔG) values were found to be negative at all temperatures

indicating the spontaneous nature of CO_2 adsorption on AC. The decrease in ΔG with increasing the temperature demonstrates that the CO_2 adsorption is exothermic and is spontaneous and more favorable at lower temperature. It must be noted that ΔG change ranges up to −20 kJ/mol indicate electrostatic interaction between sorption sites and the CO_2 molecules (physical adsorption), while for chemical adsorption it ranges between (-20 and -40) kJ/mol involve electron sharing [55]. The ΔG values obtained in this study was lower than -20 kJ/mol and therefore the adsorption was predominantly physical adsorption process.

The negative values of ΔH further confirm the exothermic nature of the adsorption process. The low enthalpy amount confirms the physisorption of the process of adsorption.Also the values of enthalpy in the ranges of surface loading of 0.2-1 were almost constant due to the homogeneous adsorption system which agreed with the results obtained from isosteric heat of absorption at a constant adsorbate loading. Negative value of change in entropy (ΔS) reflects a decrease in degree of freedom of the adsorbed species. Therefore reduction in concentration of adsorbate in solid–gas interface indicates an enhancement in adsorbate concentration onto the solid phase. As it was shown in table 7, with increasing the surface coverage -ΔS was increased due to the increasing the adsorbate concentration onto the solid phase.

3.10 Comparison of CO_2 adsorption capacity with other adsorbents

The CO_2 uptake performance of the AC sample synthesized in this work was compared to other adsorbents reported in the literature as summarized in Table 8. Based on the Table 8, it shows that there are many studies on the adsorption of CO_2 using various types of adsorbent. Nevertheless, the adsorbent capacity for each adsorbent is different due to the different type of raw material and preparation procedures of adsorbents which effect on the properties of them.

Also, it was found from Table 8 that the activated carbon prepared under optimum condition from pine cone can be more effective in CO_2 adsorption than commercial activated carbons. Therefore, it is clear that the low-cost adsorbents such as pine cone- based AC used in this study offer a lot of promising benefits for commercial purposes.

4. Conclusion

Response surface methodology was successfully used to investigate the combined effect of activation time, activation temperature, and impregnation ratio of H_3PO_4 on the optimum conditions for the preparation of activated carbon from pine cone. Desirable production outputs such as CO_2 adsorption capacity, iodine number and carbon yield were considered as responses.

The optimum preparation condition using central composite design were found to be at 170.45 min activation time, 488.82 ^{0}C activation temperature, and 2.2 impregnation ratio which resulting in 1.91 mmol/g CO_2 adsorption at 298 K and 1 bar, 1345 mg/g of iodine number and 51.17 % of carbon yield. The optimum activated carbon showed high surface area and well-developed porosity. The BET surface area and total pore volume of optimum adsorbent were 1470 m^2/g and 0.6415 cm^3/g, respectively. Isotherm and thermodynamic studies revealed that pine cone activated carbon prepared using phosphoric acid as the activating agent can be effectively employed for the adsorption of CO_2 molecules.

References

1. F. Montagnaro, A. Silvestre-Albero, J. Silvestre-Albero, F. Rodríguez-Reinoso, A. Erto, A. Lancia and M. Balsamo, Microporous and Mesoporous Materials, 2015, 209, 157-164.

2. T. D. Pham, R. Xiong, S. I. Sandler and R. F. Lobo, Microporous and Mesoporous Materials, 2014, 185, 157-166.

3. L. Zhang, Z.-Y. Qu, Y.-F. Yan, S.-X. Ju and Z.-E. Zhang, RSC Advances, 2015, 5, 424-433.

4. S. Norouzbahari, S. Shahhosseini and A. Ghaemi, Journal of Natural Gas Science and Engineering, 2015, 26, 1059-1067.

5. R. Kishor and A. K. Ghoshal, Chemical Engineering Journal, 2015, 262, 882-890.

6. G. Sethia and A. Sayari, Energy & Fuels, 2014, 28, 2727-2731.

7. J. Fujiki, H. Yamada and K. Yogo, Microporous and Mesoporous Materials, 2015, 215, 76-83.

8. R. Krupiczka, A. Rotkegel and Z. Ziobrowski, Separation and Purification Technology, 2015.

9. L. Riboldi, O. Bolland, J. M. Ngoy and N. Wagner, Energy Procedia, 2014, 63, 2289-2304.

10. B. S. Caglayan and A. E. Aksoylu, Journal of hazardous materials, 2013, 252, 19-28.

11. E. David and J. Kopac, Journal of Analytical and Applied Pyrolysis, 2014, 110, 322-332.

12. H. V. Thang, L. Grajciar, P. Nachtigall, O. Bludský, C. O. Areán, E. Frýdová and R. Bulánek, Catalysis Today, 2014, 227, 50-56.

13. S. Loganathan, M. Tikmani, S. Edubilli, A. Mishra and A. K. Ghoshal, Chemical Engineering Journal, 2014, 256, 1-8.

14. M.-S. Lee, S.-Y. Lee and S.-J. Park, International Journal of Hydrogen Energy, 2015, 40, 3415-3421.

15. D.-S. Chen, J.-M. Cheng, L.-B. Sun, Z.-Q. Liang, K.-Z. Shao, C.-G. Wang, H.-Z. Xing and Z.-M. Su, Inorganic Chemistry Communications, 2013, 38, 104-107.

16. T.-H. Liou, Chemical Engineering Journal, 2010, 158, 129-142.

17. R. Bai, M. Yang, G. Hu, L. Xu, X. Hu, Z. Li, S. Wang, W. Dai and M. Fan, Carbon, 2015, 81, 465-473.

18. A. Heidari, H. Younesi, A. Rashidi and A. Ghoreyshi, Journal of the Taiwan Institute of Chemical Engineers, 2014, 45, 579-588.

19. S. Khalili, A. A. Ghoreyshi, M. Jahanshahi and K. Pirzadeh, CLEAN–Soil, Air, Water, 2013, 41, 939-948.

20. V. K. Gupta, D. Pathania, S. Sharma and P. Singh, Journal of colloid and interface science, 2013, 401, 125-132.

21. M. Momčilović, M. Purenović, A. Bojić, A. Zarubica and M. Ranđelović, Desalination, 2011, 276, 53-59.

22. C. Djilani, R. Zaghdoudi, F. Djazi, B. Bouchekima, A. Lallam, A. Modarressi and M. Rogalski, Journal of the Taiwan Institute of Chemical Engineers, 2015, 53, 112-121.

23. N. F. Tehrani, J. S. Aznar and Y. Kiros, Journal of Cleaner Production, 2015, 91, 64-70.

24. A. C. Martins, O. Pezoti, A. L. Cazetta, K. C. Bedin, D. A. Yamazaki, G. F. Bandoch, T. Asefa, J. V. Visentainer and V. C. Almeida, Chemical Engineering Journal, 2015, 260, 291-299.

25. T. Bohli, A. Ouederni, N. Fiol and I. Villaescusa, Comptes Rendus Chimie, 2015, 18, 88-99.

26. M. Yang, L. Guo, G. Hu, X. Hu, L. Xu, J. Chen, W. Dai and M. Fan, Environmental science & technology, 2015.

27. S. Dawood, T. Sen and C. Phan, Water Air Soil Pollut, 2013, 225, 1-16.

28. N. Ferrera-Lorenzo, E. Fuente, I. Suárez-Ruiz and B. Ruiz, Fuel Processing Technology, 2014, 121, 25-31.

29. A. R. Mohamed, M. Mohammadi and G. N. Darzi, Renewable and Sustainable Energy Reviews, 2010, 14, 1591-1599.

30. S. Zuo, J. Yang, J. Liu and X. Cai, Fuel Processing Technology, 2009, 90, 994-1001.

31. V. Fierro, V. Torné-Fernández, D. Montané and A. Celzard, Thermochimica acta, 2005, 433, 142-148.

32. A. L. Cazetta, S. P. Azevedo, O. Pezoti, L. S. Souza, A. M. Vargas, A. T. Paulino, J. C. Moraes and V. C. Almeida, Journal of Analytical and Applied Pyrolysis, 2014, 110, 455-462.

33. M. A. Bezerra, R. E. Santelli, E. P. Oliveira, L. S. Villar and L. A. Escaleira, Talanta, 2008, 76, 965-977.

34. A. M. Vargas, C. A. Garcia, E. M. Reis, E. Lenzi, W. F. Costa and V. C. Almeida, Chemical Engineering Journal, 2010, 162, 43-50.

35. J. Sahu, J. Acharya and B. Meikap, Bioresource technology, 2010, 101, 1974-1982.

36. Z.-Y. Zhong, Q. Yang, X.-M. Li, K. Luo, Y. Liu and G.-M. Zeng, Industrial Crops and Products, 2012, 37, 178-185.

37. M. T. Yagub, T. K. Sen, S. Afroze and H. M. Ang, Advances in colloid and interface science, 2014, 209, 172-184.

38. M. A. Ahmad and R. Alrozi, Chemical Engineering Journal, 2011, 171, 510-516.

39. R. Chaudhary and S. Mayadevi, Zeolites, 1996, 17, 501-507.

40. P. Tripathi, V. C. Srivastava and A. Kumar, Desalination, 2009, 249, 1273-1279.

41. A. Arami-Niya, W. M. A. W. Daud, F. S. Mjalli, F. Abnisa and M. S. Shafeeyan, Chemical engineering research and design, 2012, 90, 776-784.

42. D. Li, R. Tang, Y. Tian, Y. Qiao and J. Li, BioResources, 2014, 9, 1246-1254.

43. R. C. Bansal and M. Goyal, Activated carbon adsorption, CRC press, 2005.

44. M. Loredo-Cancino, E. Soto-Regalado, F. Cerino-Córdova, R. García-Reyes, A. García-León and M. Garza-González, Journal of environmental management, 2013, 125, 117-125.

45. Z.-Y. Zhong, Q. Yang, X.-M. Li, K. Luo, Y. Liu and G.-M. Zeng, Industrial Crops and Products, 2012, 37, 178-185.

46. A. C. Lua, T. Yang and J. Guo, Journal of analytical and applied pyrolysis, 2004, 72, 279-287.

47. B. S. Girgis, S. S. Yunis and A. M. Soliman, Materials Letters, 2002, 57, 164-172.

48. N. B. Azmi, M. J. Bashir, S. Sethupathi, L. J. Wei and N. C. Aun, Journal of Environmental Chemical Engineering, 2015, 3, 1287–1294.

49. A. Barroso-Bogeat, M. Alexandre-Franco, C. Fernández-González, A. Macías-García and V. Gómez-Serrano, Microporous and Mesoporous Materials, 2015, 209, 90-98.

50. C. Saka, Journal of Analytical and Applied Pyrolysis, 2012, 95, 21-24.

51. H. Jin, Y. S. Lee and I. Hong, Catalysis today, 2007, 120, 399-406.

52. S.-Y. Lee and S.-J. Park, Journal of colloid and interface science, 2013, 389, 230-235.

53. M. Cinke, J. Li, C. W. Bauschlicher, A. Ricca and M. Meyyappan, Chemical Physics Letters, 2003, 376, 761-766.

54. V. C. Srivastava, I. D. Mall and I. M. Mishra, Chemical Engineering Journal, 2007, 132, 267-278.

55. T. Anirudhan and P. Radhakrishnan, Chemical Engineering Journal, 2010, 165, 142-150.

56. H. Yang, M. Gong and Y. Chen, Journal of Natural Gas Chemistry, 2011, 20, 460-464.

57. C. Lee, Y. Ong, M. Aroua and W. W. Daud, Chemical Engineering Journal, 2013, 219, 558-564.

58. Z.-S. Liu, Y.-H. Peng, C.-Y. Huang and M.-J. Hung, Thermochimica Acta, 2015, 602, 8-14.

59. R. Kishor and A. K. Ghoshal, Chemical Engineering Journal, 2015, 262, 882-890.

60. T. Watabe and K. Yogo, Separation and Purification Technology, 2013, 120, 20-23.

61. E. S. Sanz-Pérez, M. Olivares-Marín, A. Arencibia, R. Sanz, G. Calleja and M. M. Maroto-Valer, International Journal of Greenhouse Gas Control, 2013, 17, 366-375.

62. R. Chatti, A. K. Bansiwal, J. A. Thote, V. Kumar, P. Jadhav, S. K. Lokhande, R. B. Biniwale, N. K. Labhsetwar and S. S. Rayalu, Microporous and Mesoporous Materials, 2009, 121, 84-89.

63. X. Xu, X. Zhao, L. Sun and X. Liu, Journal of Natural Gas Chemistry, 2009, 18, 167-172.

64. Y. Lin, Q. Yan, C. Kong and L. Chen, Scientific reports, 2013, 3, 1-7.

65. D. P. Bezerra, R. S. Oliveira, R. S. Vieira, C. L. Cavalcante Jr and D. C. Azevedo, Adsorption, 2011, 17, 235-246.

66. M. S. Shafeeyan, W. M. A. W. Daud, A. Houshmand and A. Arami-Niya, Applied Surface Science, 2011, 257, 3936-3942.

67. C. Pevida, M. Plaza, B. Arias, J. Fermoso, F. Rubiera and J. Pis, Applied Surface Science, 2008, 254, 7165-7172.

68. B. S. Caglayan and A. E. Aksoylu, Journal of hazardous materials, 2013, 252, 19-28.

Table 1 Experimental design matrix and results

Run no.	Time (min)		Temperature(^{0}C)		Impregnation ratio		CO_2 adsorption, Y_1(mmol/g)		Iodine number, Y_2(mg/g)		Carbon Yield, Y_3 (%)	
	X_1		X_2		X_3							
	Coded	Actual	Coded	Actual	Coded	Actual	Observed	Predicted	Observed	Predicted	Observed	Predicted
1	0	120	0	550	-1.68	0.66	2.11	2.06	1262	1270	50.67	50.66
2	0	120	0	550	1.68	2.34	1.22	1.26	1309	1302	54.86	54.20
3	0	120	1.68	718.18	0	1.5	1.25	1.29	1369	1378	45.67	44.61
4	0	120	-1.68	381.82	0	1.5	1.19	1.14	1379	1372	48.86	49.24
5	1.68	170.45	0	550	0	1.5	1.26	1.22	1346	1341	52.29	52.90
6	-1.68	69.55	0	550	0	1.5	0.86	0.89	1264	1271	59.43	58.14
7	1	150	-1	450	1	2	1.46	1.49	1345	1353	51.67	51.22
8	-1	90	1	650	-1	1	1.88	1.86	1305	1296	48.55	49.48
9	-1	90	-1	450	-1	1	1.26	1.30	1274	1270	57.29	57.37
10	1	150	1	650	1	2	1.15	1.11	1332	1335	53.2	53.60
11	1	150	1	650	-1	1	1.51	1.55	1345	1340	47.17	47.05
12	1	150	-1	450	-1	1	1.53	1.57	1342	1345	47.71	47.23
13	-1	90	1	650	1	2	1.01	0.98	1330	1326	48.75	49.70
14	-1	90	-1	450	1	2	0.81	0.78	1309	1313	54.43	55.03
15	0	120	0	550	0	1.5	0.88	0.95	1325	1320	56.57	56.42
16	0	120	0	550	0	1.5	0.86	0.95	1317	1320	55.86	56.42
17	0	120	0	550	0	1.5	0.96	0.95	1317	1320	56.01	56.42
18	0	120	0	550	0	1.5	1.06	0.95	1322	1320	55.78	56.42
19	0	120	0	550	0	1.5	1.01	0.95	1320	1320	56.53	56.42
20	0	120	0	550	0	1.5	0.92	0.95	1318	1320	57.65	56.42

Table 2 Ultimate and proximate analysis of pine cone and prepared activated carbon.

Sample	Ultimate analysis					Proximate analysis			
	Carbon	Hydrogen	Nitrogen	Sulfur	*Oxygen	Moisture	Volatile matter	Ash	*Fixed carbon
Pine cone	47.71	6.16	0.12	1.21	44.80	9.63	79.05	2.21	9.11
AC	71.32	4.30	0.00	0.90	23.48	6.50	22.04	3.75	67.71

* Calculated by difference

Table 3 Analysis of variance (ANOVA) for the fitted quadratic polynomial models.

Source	Sum of squares			Degree of freedom	Mean square			F-value			Prob > F		
	CO_2 (Y_1)	I_2 (Y_2)	Yield (Y_3)		CO_2 (Y_1)	I_2 (Y_2)	Yield (Y_3)	CO_2 (Y_1)	I_2 (Y_2)	Yield (Y_3)	CO_2 (Y_1)	I_2 (Y_2)	Yield (Y_3)
Model	2.239	17019.26	306.536	9	0.249	1891.029	34.060	50.834	31.219	38.237	< 0.0001	< 0.0001	< 0.0001
X_1	0.136	5902.032	33.152	1	0.136	5902.032	33.152	27.790	97.435	37.219	0.0004	< 0.0001	0.0001
X_2	0.026	46.434	25.866	1	0.026	46.434	25.866	5.225	0.767	29.039	0.0453	0.4018	0.0003
X3	0.772	1219.345	15.135	1	0.772	1219.345	15.135	157.757	20.130	16.991	< 0.0001	0.0012	0.0021
X_1X_2	0.165	480.5	29.684	1	0.165	480.500	29.684	33.786	7.932	33.325	0.0002	0.0183	0.0002
X_1X_3	0.099	612.5	20.003	1	0.099	612.500	20.003	20.236	10.112	22.456	0.0011	0.0098	0.0008
X_2X_3	0.063	84.5	3.290	1	0.063	84.500	3.290	12.878	1.395	3.693	0.0049	0.2649	0.0836
X_1^2	0.020	360.560	1.449	1	0.020	360.560	1.449	4.067	5.952	1.627	0.0714	0.0349	0.2310
X_2^2	0.127	5420.062	162.300	1	0.127	5420.062	162.300	25.875	89.479	182.208	0.0005	< 0.0001	< 0.0001
X_3^2	0.908	2039.487	28.706	1	0.908	2039.487	28.706	185.648	33.669	32.227	< 0.0001	0.0002	0.0002
Residual	0.049	605.738	8.907	10	0.005	60.574	0.891						
Lack of fit	0.019	554.905	6.471	5	0.004	110.981	1.294	0.648	10.92	2.66	0.6770	0.0101	0.1537
Pure error	0.030	50.833	2.436	5	0.006	10.167	0.487						
Cor Total	2.287	17625	315.443	19									
			For CO_2 Asorption:		R^2 = 0.9786;		adjusted R^2 = 0.9594;			adequate precision = 25.778			
			For I_2 Asorption:		R^2 = 0.9656;		adjusted R^2 = 0.9347;			adequate precision = 19.532			
			For Carbon Yield:		R^2 = 0.9718;		adjusted R^2 = 0.9463;			adequate precision = 20.274			

Table 4 Process optimization validation.

Activation time, X_1 (min)	Activation temperature, X_2 (^{0}C)	Chemical ratio, X_3	CO_2 adsorption (mmol/g)		Iodine number (mg/g)		Carbon yield (%)	
			Predicted	Experimental	Predicted	Experimental	Predicted	Experimental
170.45	488.82	2.2	1.88	1.91	1327	1345	52.39	51.17

Table 5 Textural properties of optimum sample

BET surface area (m^2/g)	1470
Total pore volume (cm^3/g)	0.6415
Micropore volume (cm^3/g)	0.6304
Mesopore volume(cm^3/g)	0.0111
Micropore volume (%)	98
Average pore diameter (nm)	1.7452
Micropore width(nm)	0.7572

Table 6 Langmuir and Freundlich isotherm constants for adsorption of CO_2 on AC.

Temperature (K)	Langmuir			Freundlich		
	b	q_m(mmol/g)	R^2	K	n	R^2
298	0.258	9.464	0.999	2.325	2.260	0.978
308	0.196	8.641	0.999	1.826	2.106	0.982
318	0.157	8.218	0.998	1.444	1.922	0.984

Table7 Thermodynamic parameters for CO_2 adsorption onto prepared AC

q_e(mmol/g)	ΔS(J/mol K)	ΔG(kJ/mol)			ΔH(kJ/mol)
		298	308	318	
0.2	-76.2	-5.780	-5.109	-4.255	-28.533
0.4	-79.4	-4.012	-3.278	-2.423	-27.708
0.6	-83.0	-3.101	-2.221	-1.440	-27.833
0.8	-85.5	-2.333	-1.439	-0.623	-27.799
1	-85.7	-1.767	-0.806	-0.053	-27.271

Table 8 Comparison of CO_2 adsorption capacity with other adsorbents.

Adsorbent	Surface Area ($m^2.g^{-1}$)	Adsorption Capacity($mmol.g^{-1}$)	Pressure(bar)	Temperature(K)	Refs.
Coconut shell- based AC	1922	2.55	2	298	56
Palm shell- based AC	882	0.8	1	313	57
Activated carbon fiber	1223	0.04	1	303	58
KIT-6 silica	711	0.48	1	303	59
MSU-H silica	744	0.5	1	313	60
SBA-15 silica	587	0.32	1	298	61
X-zeolite	386	0.36	1	298	62
β-zeolite	574	1.76	1	303	63
MOF	3125	1.6	1	298	64
MWCNT	272	0.55	1	298	14
Commercial AC	1727	1.89	1	298	65
Commercial AC	768	1.14	1	303	66
Commercial AC	1361	1.59	1	298	67
Commercial AC	1190	1.22	1	at room temperature	68
Pine cone- based AC	1470	1.91	1	298	This study

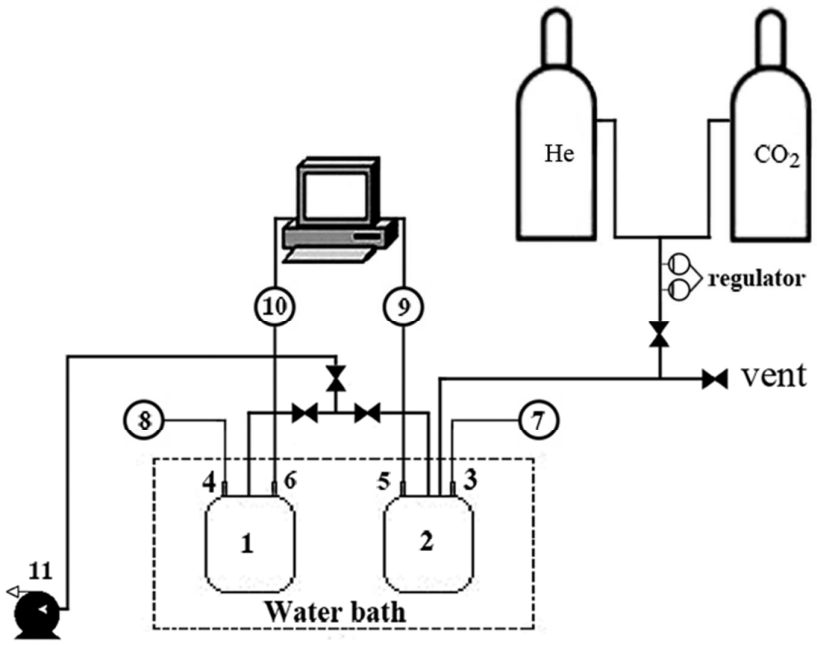

Fig.1 Schematic diagram of the volumetric adsorption apparatus: (1) pressure cell; (2) sample cell; (3, 4) temperature probe; (5, 6) pressure transducer; (7, 8) temperature digital indicator; (9, 10) pressure digital indicator; (11) vacuum pump.

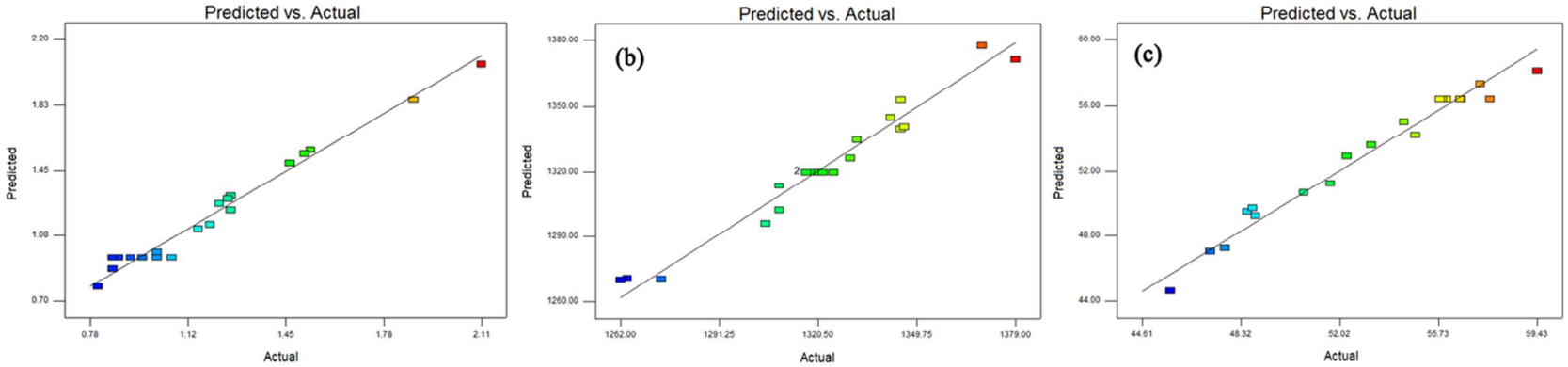

Fig. 2 Predicted vs. experimental values of CO_2 adsorption (a), iodine number (b) and carbon yield (c).

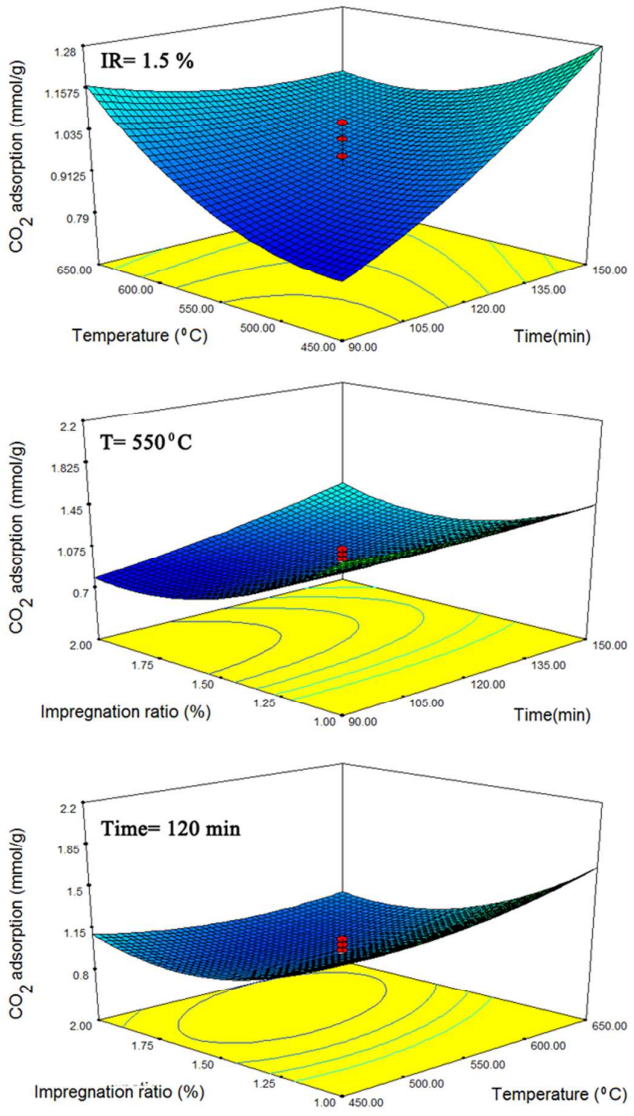

Fig.3 Three-dimensional standard error plot for adsorption of CO_2 by AC

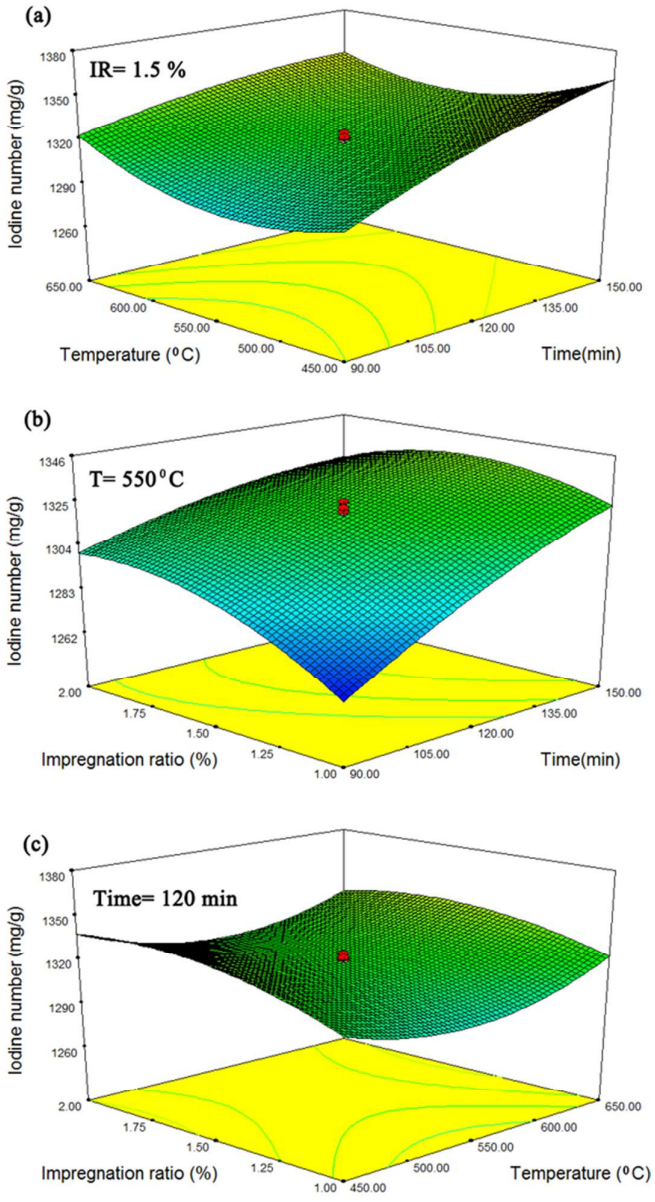

Fig.4 Three-dimensional standard error plot for Iodine number by AC.

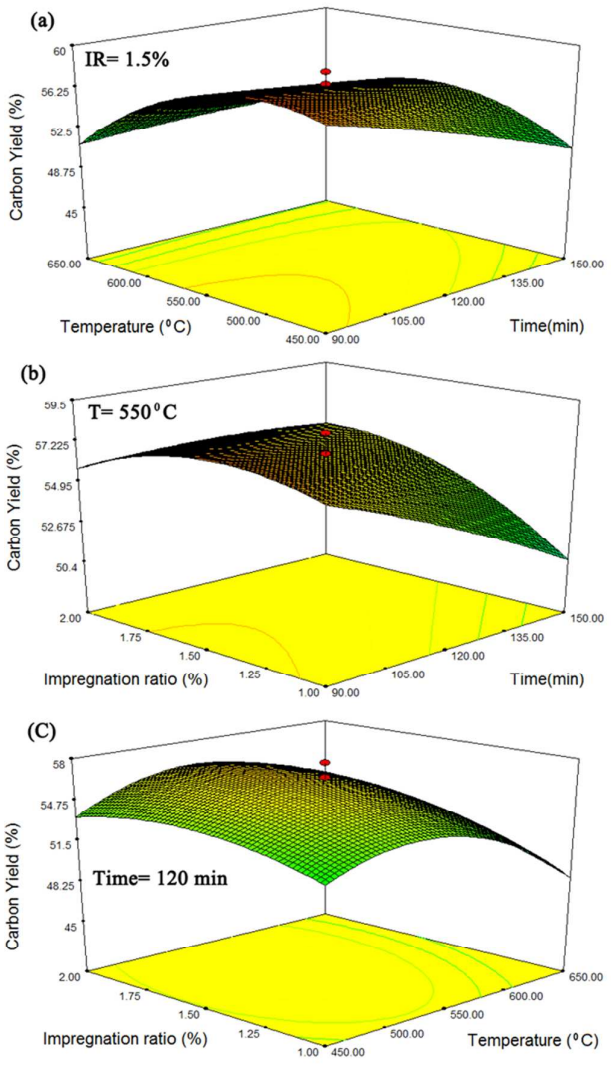

Fig.5 Three-dimensional standard error plot for carbon yield

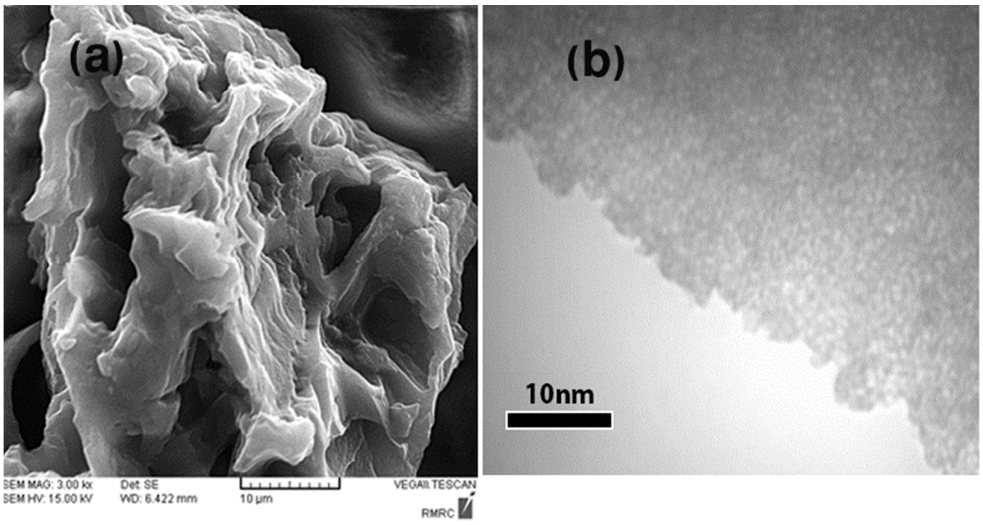

Fig.6 SEM (a) and TEM (b) images of prepared activated carbon.

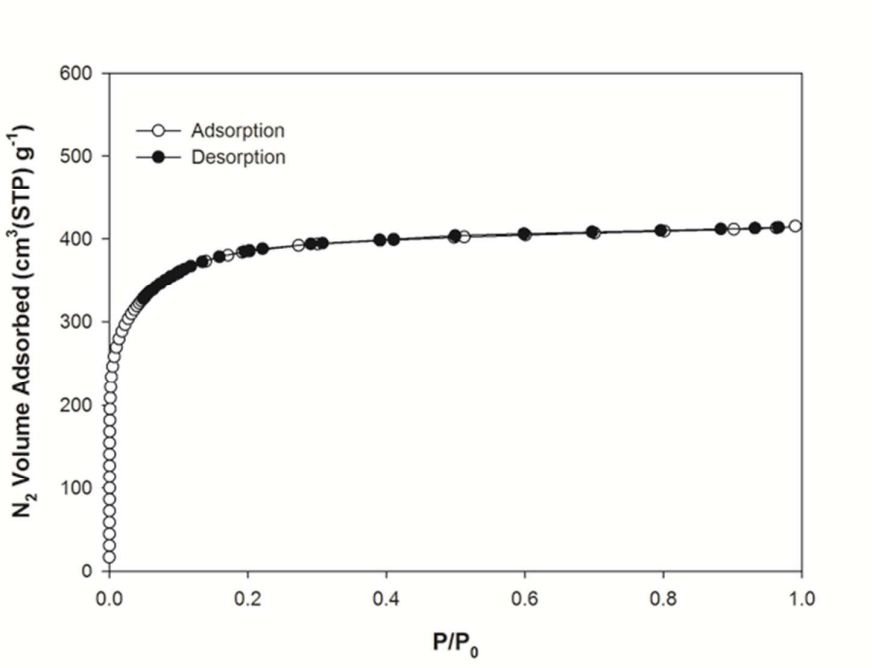

Fig. 7 Adsorption/desorption isotherms of N_2 for AC.

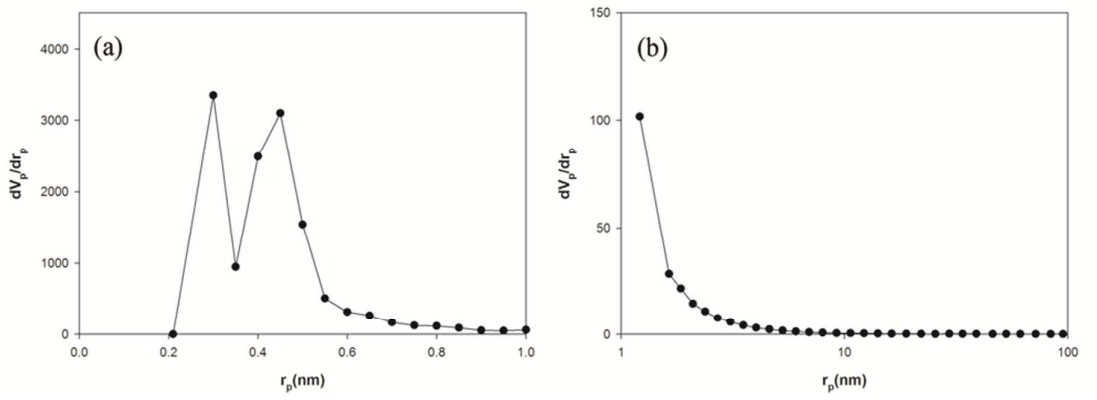

Fig. 8 Micropore (a) and mesopore (b) size distributions of AC obtained by MP and BJH.

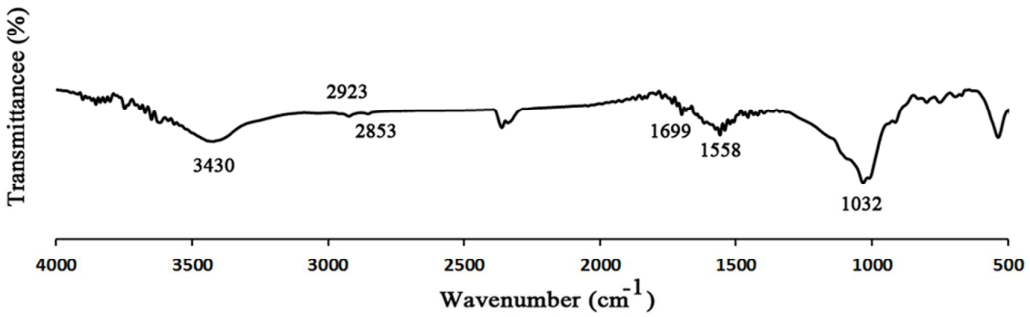

Fig. 9 FTIR spectra for the AC sample derived from Pine cone

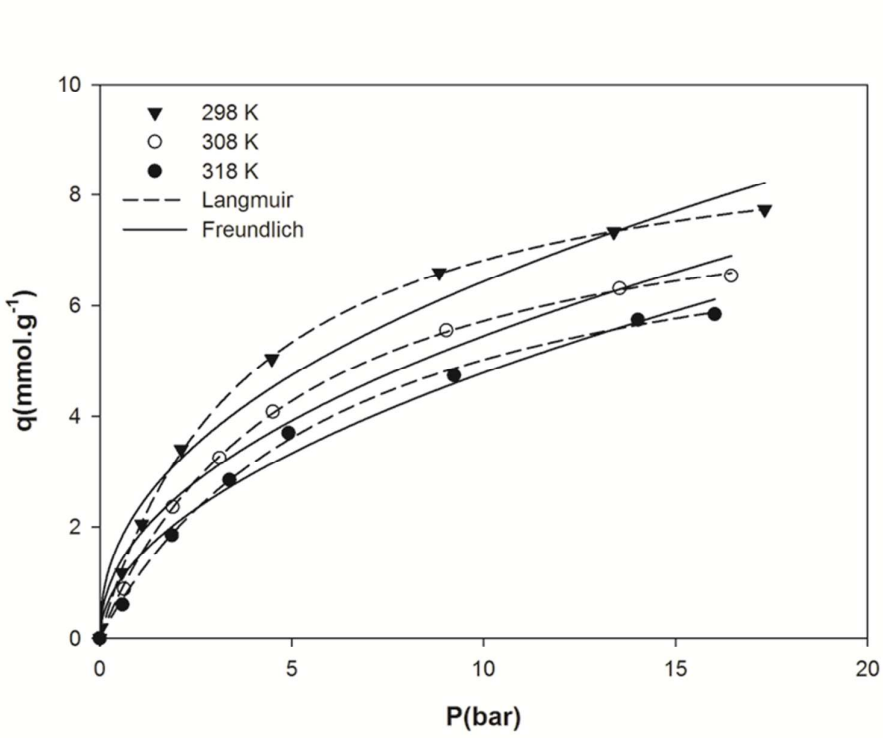

Fig.10 CO_2 adsorption isotherm for AC at different temperatures and nonlinear fit of experimental data with Langmuir and Freundlich models

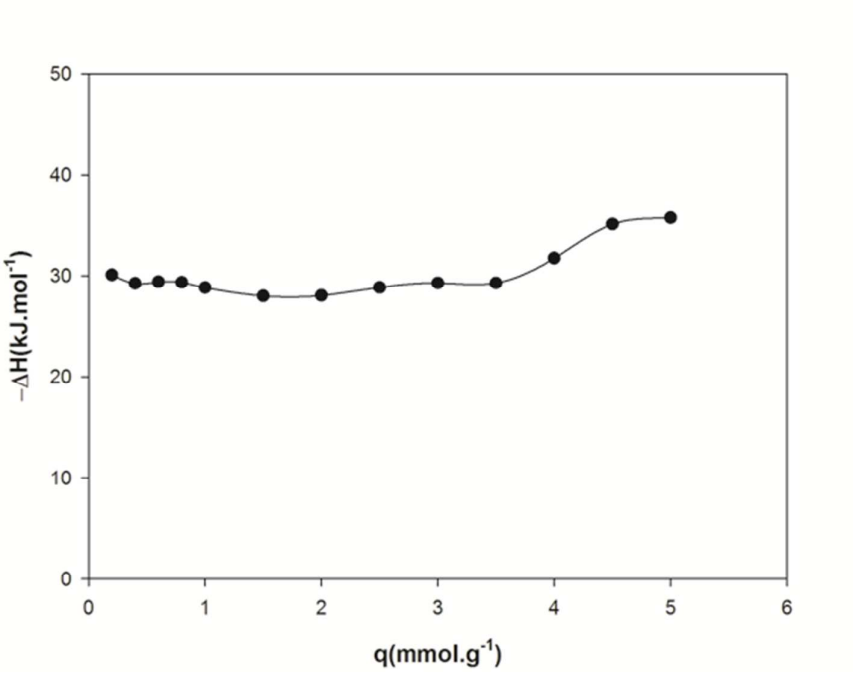

Fig. 11 Isosteric heat of adsorption against surface loading for adsorption of CO_2 onto AC.